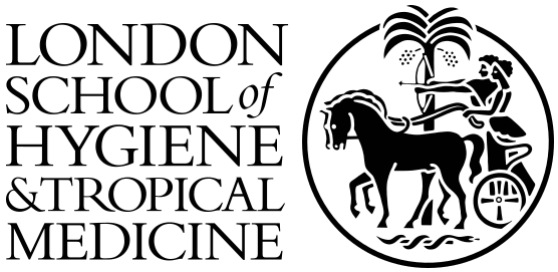

AMERICAN SOCIETY FOR MICROBIOLOGY | mBio®

RESEARCH ARTICLE
Molecular Biology and Physiology

# Deletion of *Plasmodium falciparum* Protein RON3 Affects the Functional Translocation of Exported Proteins and Glucose Uptake

**Leanne M. Low,[a] Yvonne Azasi,[a] Emma S. Sherling,[a,b] Matthias Garten,[c] Joshua Zimmerberg,[c] Takafumi Tsuboi,[d] Joseph Brzostowski,[e] Jianbing Mu,[a] Michael J. Blackman,[b,f] Louis H. Miller[a]**

[a]Laboratory of Malaria and Vector Research, National Institute of Allergy and Infectious Diseases, NIH, Rockville, Maryland, USA
[b]Malaria Biochemistry Laboratory, The Francis Crick Institute, London, United Kingdom
[c]Section on Integrative Biophysics, Eunice Kennedy Shriver National Institute of Child Health and Human Development, NIH, Bethesda, Maryland, USA
[d]Division of Malaria Research, Proteo-Science Center, Ehime University, Matsuyama, Ehime, Japan
[e]LIG Imaging Facility, NIAID, NIH, Rockville, Maryland, USA
[f]Faculty of Infectious and Tropical Diseases, London School of Hygiene & Tropical Medicine, London, United Kingdom

**ABSTRACT** The survival of *Plasmodium* spp. within the host red blood cell (RBC) depends on the function of a membrane protein complex, termed the *Plasmodium* translocon of exported proteins (PTEX), that exports certain parasite proteins, collectively referred to as the exportome, across the parasitophorous vacuolar membrane (PVM) that encases the parasite in the host RBC cytoplasm. The core of PTEX consists of three proteins: EXP2, PTEX150, and the HSP101 ATPase; of these three proteins, only EXP2 is a membrane protein. Studying the PTEX-dependent transport of members of the exportome, we discovered that exported proteins, such as ring-infected erythrocyte surface antigen (RESA), failed to be transported in parasites in which the parasite rhoptry protein RON3 was conditionally disrupted. RON3-deficient parasites also failed to develop beyond the ring stage, and glucose uptake was significantly decreased. These findings provide evidence that RON3 influences two translocation functions, namely, transport of the parasite exportome through PTEX and the transport of glucose from the RBC cytoplasm to the parasitophorous vacuolar (PV) space where it can enter the parasite via the hexose transporter (HT) in the parasite plasma membrane.

**IMPORTANCE** The malarial parasite within the erythrocyte is surrounded by two membranes. *Plasmodium* translocon of exported proteins (PTEX) in the parasite vacuolar membrane critically transports proteins from the parasite to the erythrocytic cytosol and membrane to create protein infrastructure important for virulence. The components of PTEX are stored within the dense granule, which is secreted from the parasite during invasion. We now describe a protein, RON3, from another invasion organelle, the rhoptry, that is also secreted during invasion. We find that RON3 is required for the protein transport function of the PTEX and for glucose transport from the RBC cytoplasm to the parasite, a function thought to be mediated by PTEX component EXP2.

**KEYWORDS** PTEX, malaria, parasite proteins, parasitophorous vacuolar space

Malaria is a deadly infectious disease caused by parasites of *Plasmodium* spp. that in the asexual phase of their life cycle infect and replicate within red blood cells (RBCs). In a *Plasmodium*-infected RBC, the parasite is surrounded by the parasitophorous vacuolar membrane (PVM) that forms initially from the erythrocyte membrane during parasite invasion (1). The RBC has little biosynthetic capacity, and for essential

**Citation** Low LM, Azasi Y, Sherling ES, Garten M, Zimmerberg J, Tsuboi T, Brzostowski J, Mu J, Blackman MJ, Miller LH. 2019. Deletion of *Plasmodium falciparum* protein RON3 affects the functional translocation of exported proteins and glucose uptake. mBio 10:e01460-19. https://doi.org/10.1128/mBio.01460-19.

**Editor** L. David Sibley, Washington University School of Medicine



Address correspondence to Louis H. Miller, lmiller@niaid.nih.gov.

L.M.L., Y.A., and E.S.S. contributed equally to this work.

This article is a direct contribution from a Fellow of the American Academy of Microbiology. Solicited external reviewers: Tania de Koning-Ward, Deakin University; Brendan Crabb, Burnet Institute; Paul Gilson, Burnet Institute.

**Received** 10 June 2019
**Accepted** 13 June 2019
**Published** 9 July 2019

functions, the parasite must export a subset of its own proteins, termed the exportome, across the PVM into the RBC cytoplasm and to the RBC membrane. These transported proteins are needed to build the protein infrastructure required for parasite functions essential for their pathological survival in the vertebrate host, including remodeling of the RBC membrane to express receptors for endothelial ligands that sequester infected RBCs in host tissue, thereby avoiding elimination by the spleen. Protein export across the PVM involves ATP-dependent protein unfolding and transport; this process is mediated by a channel assembled in the PVM referred to as the *Plasmodium* translocon of exported proteins (PTEX) (2). The core components of PTEX are heat shock protein 101 (HSP101) ATPase, which can unfold proteins, and a transmembrane funnel comprised of oligomeric exported protein 2 (EXP2) and PTEX150; genetic interference of any one of the three PTEX components destroys its function (3, 4). Independent of these discoveries is the identification of a sequence in the N termini of exportome proteins called the *Plasmodium* export element (PEXEL) or host-targeting (HT) motif that is recognized by an aspartic protease, plasmepsin V; this has been shown to clip off the motif before the protein destined for export associates with PTEX (5, 6). However, the PEXEL motif is not always required for export, as evidenced by exported proteins lacking a PEXEL motif (termed PEXEL-negative exported proteins or PNEPs) (7). A major advance in understanding the mechanism of protein transport by PTEX is the recent structural determination by cryo-electron microscopy of a purified PTEX complex that included EXP2, HSP101 ATPase, and PTEX150 (8). This purified PTEX complex, in both an "engaged" state and a "resetting" state, shows EXP2 forming a transmembrane funnel-shaped protein-conducting channel tethered to the HSP101 ATPase that powers protein translocation by a ratchet-like translocation mechanism. These findings elegantly confirmed that PTEX was indeed the site of parasite proteins passing from the parasitophorous vacuolar (PV) space to the erythrocyte cytoplasm.

Parasite metabolism within the infected RBC also requires the import of nutrients across the PVM. A nutrient-permeable channel in the PVM proposed to facilitate passage of nutrients of size as large as ~1,400 daltons from the RBC into the PV space was first described by Desai and colleagues (9, 10). Recent studies identify EXP2 as such a channel, permeable to both amino acids and glucosamine (11). However, EXP2 also functions independently of HSP101 ATPase activity, indicating that the EXP2 nutrient-permeable channel complex may not be identical to the EXP2-PTEX channel. Indeed, there is little precedent for channels that function to transport both proteins and nutrients. It is possible that EXP2 functions alone, in a complex with PTEX, or with non-PTEX components to transport nutrients.

In the present study, we describe the surprising finding that a conditional knockout (KO) of the misnamed rhoptry neck protein 3 (RON3) caused the early death of the parasite with an inability of ring-infected erythrocyte surface antigen (RESA), a protein in the dense granule, to be transported across the PVM into the RBC cytoplasm. In addition, import of glucose across the PVM to the parasite was significantly decreased in RON3-deficient parasites. RON3 is a protein found in the body of the rhoptries, not within the rhoptry neck as suggested by the name (12, 13), and is secreted into the space around the parasite during invasion. The RON3 sequence contains a signal sequence and three predicted transmembrane sequences, two of which are closely apposed and one further C-terminal (see Fig. S1 in the supplemental material) (12). All three transmembrane sequences include a single positively charged residue that may reflect a special role for RON3.

## RESULTS

To investigate the role of RON3 in the *Plasmodium falciparum* life cycle, we conditionally disrupted the gene in the 3D7 parasite clone 1G5DC using the dimerizable P1 bacteriophage cyclization recombination (DiCre) recombinase system (14). Two forms of *RON3loxP* were created by clustered regularly interspaced short palindromic repeat (CRISPR)/CRISPR-associated protein-9 (Cas9)-mediated gene editing, whereby the locus of X-over P1 (loxP) sites were inserted into different segments of the *RON3* gene. The

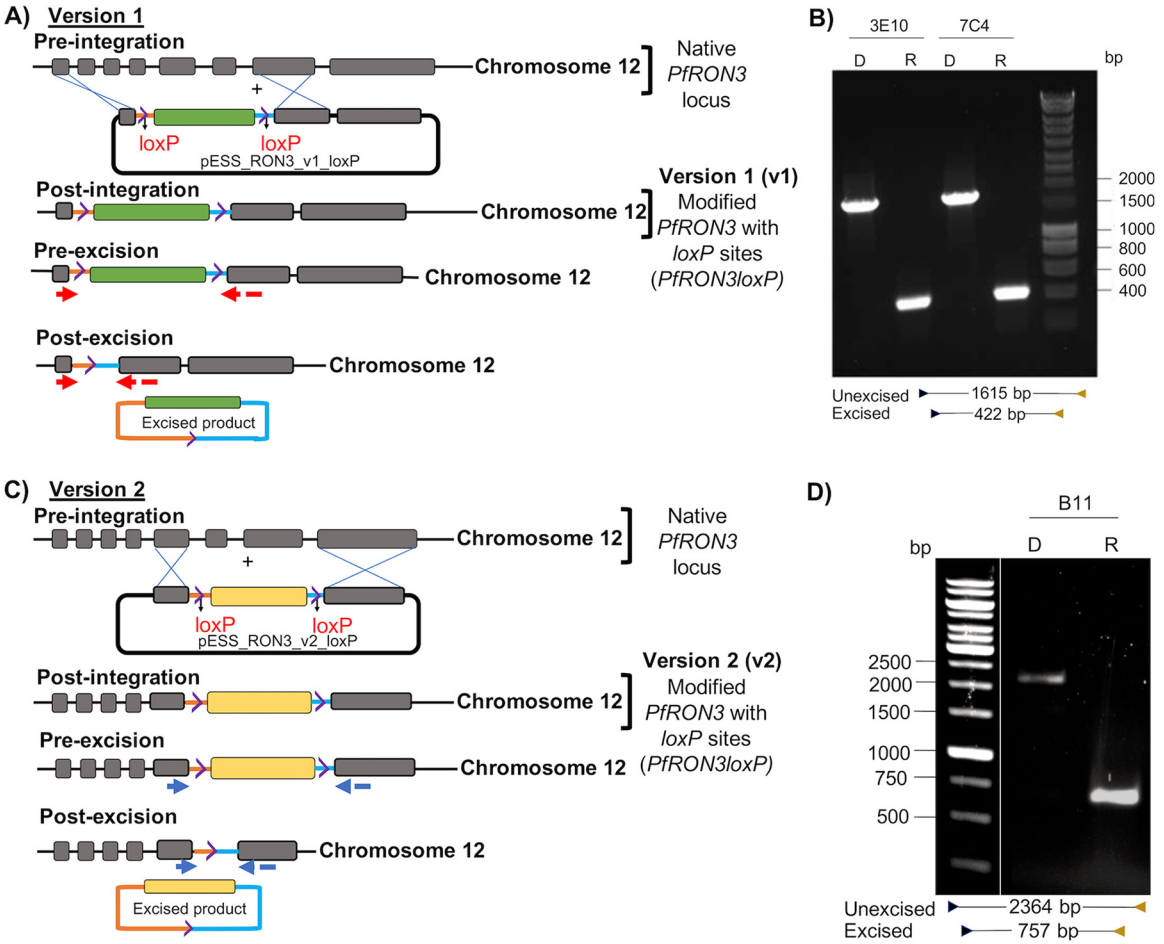


**FIG 1** Rapid and efficient conditional disruption of the *P. falciparum RON3* gene. The native *PfRON3* gene on chromosome 12 comprises 8 exons (indicated as gray boxes) and 7 introns. (A) Version 1 (v1). Schematic representation of pre- and postintegration events after CRISPR-Cas9 editing to produce the modified *RON3loxP* and the expected locus architecture before and after rapamycin treatment (pre- and postexcision). Recodonized exons 2 to 6 are shown as a green box. Red arrows indicate target areas of primers RON3_exon1_F (solid arrow)/RON3_exon7_R (dashed arrow). (B) PCR *RON3loxP* v1 clones 3E10 and 7C4 were treated with DMSO (D) or rapamycin (R), and schizonts were analyzed ~44 h after treatment to determine excision. DNA markers (M) ranged from 200 to 10,000 bp. Excision leads to a decrease in amplicon size from 1,615 bp to 422 bp. (C) Version 2 (v2). Schematic representation of pre- and postintegration events after CRISPR-Cas9 editing to produce the modified *RON3loxP* and the expected locus architecture before and after rapamycin treatment (pre- and postexcision). Recodonized exons 6 to 7 are shown as a yellow box. Blue arrows indicate target areas of primers RON3_exon4_F (solid arrow)/RON3_exon8_R (dashed arrow). (D) PCR *RON3loxP* v2 clone B11 was treated with DMSO (D) or rapamycin (R); excision leads to s decrease in amplicon size from 2,364 bp to 757 bp. DNA markers (M) ranged from 250 to 10,000 bp. Samples were run in duplicate on the same gel, with the white line indicating splicing of the image to show only one replicate.

*RON3* gene contains eight exons with the signal sequence located in exon 1. For version 1 (v1), the *RON3* gene was modified such that exons 2 to 6 were recodonized without introns between them. This was flanked by synthetic introns containing loxP sites (Fig. 1A). In version 2 (v2), *RON3* was edited further toward the 3′ end of the gene by replacing exons 6 to 7 with a recodonized version containing no introns. The endogenous introns on either side of exons 6 to 7 were replaced with synthetic loxP-containing introns (Fig. 1C).

Disruption of the *RON3* gene was induced in ring-stage parasites; excision of the gene is mediated by brief rapamycin treatment, allowing the activation of the Cre recombinase that recognizes loxP sequences by dimerization of the DiCre components (14). Rapamycin treatment was predicted to lead to the excision of the recodonized exons. In v1, this would eliminate the first two transmembrane domains, while in v2, this would lead to excision of the third transmembrane domain. Diagnostic PCR, using DNA extracted from dimethyl sulfoxide (DMSO)- or rapamycin-treated v1 (clones 3E10 and 7C4) and v2 (clone B11), showed the expected loss of the intervening recodonized

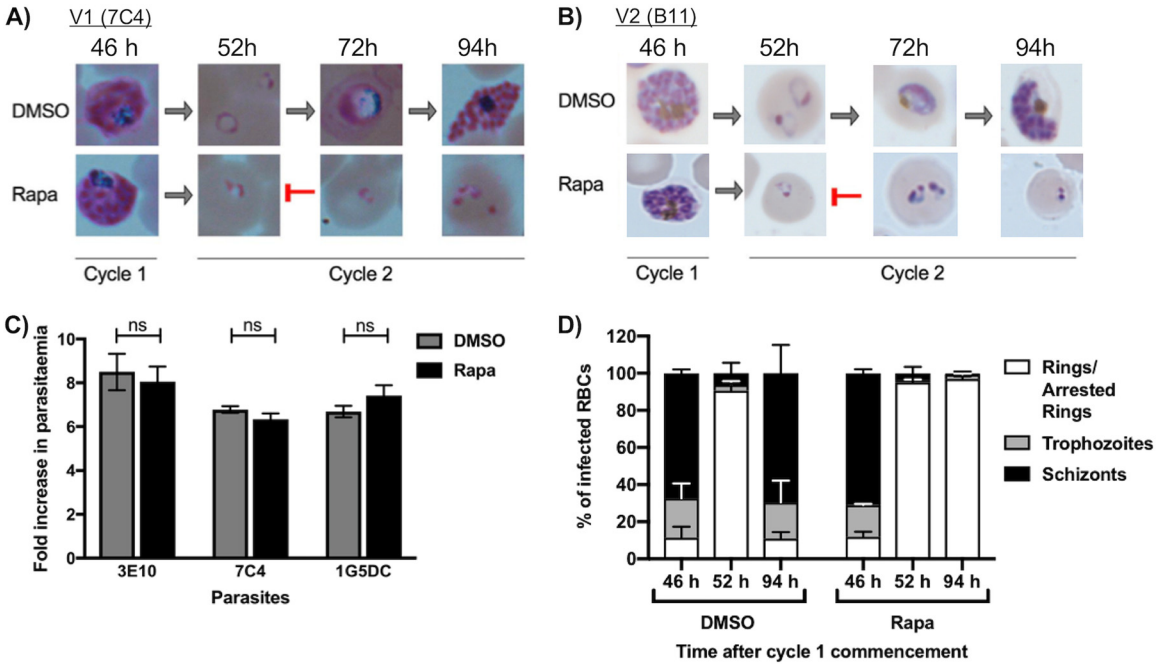


**FIG 2** RON3-deficient parasites invade normally but stall at the ring stage. (A and B) Version 1 (v1) clone 7C4 (A) or version 2 (v2) clone B11 (B) parasites were treated with DMSO or rapamycin (Rapa) for 4 h during ring stage and allowed to mature and progress into the next cycle. Microscopic images of Giemsa-stained thin blood smears were taken at 46 h, 52 h, 72 h, and 94 h following the commencement of cycle 1. Images are representative of at least three independent experiments. (C) v1 clones 7C4 and 3E10 and the parental line, 1G5DC, were treated with DMSO or rapamycin to investigate invasive capacity after loss of RON3. Schizonts were purified after treatment and allowed to undergo egress and invasion into fresh RBCs for 4 h before ring-stage parasitemia was determined by flow cytometry. Data were averaged from three biological replicate experiments, using blood samples from different donors. Values are means ± 1 standard deviation (error bars). Statistical significance was determined by a two-tailed *t* test where $P > 0.05$ is considered nonsignificant (ns). (D) Differential count of the DMSO- or rapamycin-treated v2 B11 parasite blood stages (rings, trophozoites, or schizonts) at 46 h, 52 h, and 94 h. Percentages of each blood stage (rings, trophozoites, or schizonts) were normalized to total percentage parasitemia at each time point. Data represent two independent experiments, and error bars depict standard deviations (SD).

sequence (Fig. 1B and D); v2 parasites were further sequenced, confirming the excision after rapamycin treatment and demonstrating efficient excision of the floxed sequences (data not shown).

Rapamycin-treated v1 or v2 parasites were observed to progress normally through the cycle in which they were treated (cycle 1; Fig. 2A and B). However, following invasion into cycle 2, rapamycin-treated parasites did not develop beyond the ring stage (Fig. 2A, B, and D). Comparison of ring-stage parasites at 94 h was found to be significantly different between treatment conditions ($P < 0.001$). Examination of the invasion capacity of v1 parasites (clones 3E10 and 7C4) found that rapamycin-treated parasites invaded new RBCs at a similar rate to DMSO-treated parasites of the same clone (Fig. 2C). The parental parasite clone, 1G5DC, was also included in these experiments to assess whether rapamycin treatment itself could affect invasion; this confirmed that there were no significant differences between DMSO and rapamycin treatment as previously shown (14). To rule out any effects of loxP insertion, growth rates were compared between v1 parasites and the parental clone (1G5DC) with no significant differences observed ($P > 0.05$; see Fig. S2 in the supplemental material).

To seek insights into the development defect in cycle 2 rings derived from the rapamycin-treated *RON3loxP* parasites, we examined the fate of the PTEX exported proteins RESA, knob-associated histidine-rich protein (KAHRP), and Maurer's cleft-associated histidine-rich protein 1 (MAHRP1) (Fig. 3); RESA was of particular interest, as it is known to be exported early during ring stages (15). In DMSO-treated *RON3loxP* parasites, RESA was found distributed throughout the infected RBC, concentrating in the space below the RBC membrane, as is normal (16, 17). In contrast, in newly formed rings of both v1 and v2 excised parasites, RESA was found surrounding the parasite,

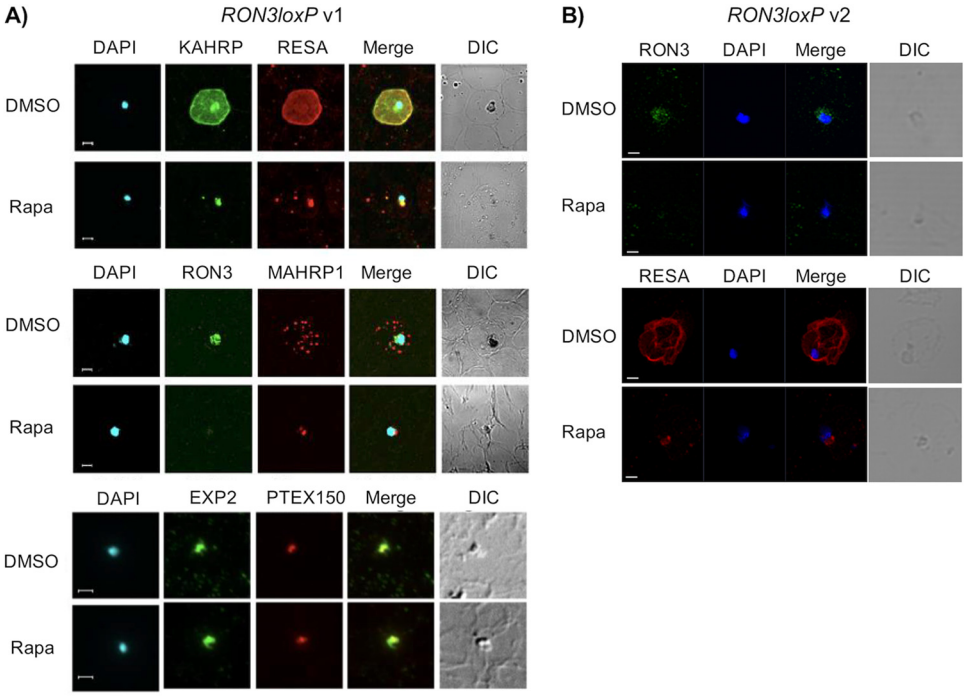


**FIG 3** RON3 is essential for the export of proteins into the infected RBC. Ring infected RBCs from *RON3loxP* v1 (A) and v2 (B) parasites were treated with DMSO or rapamycin (Rapa) for 4 h, washed, and cultured in cRPMI for ~40 to 44 h. The parasites were fixed and stained with antibodies to RON3, KAHRP, RESA, MAHRP1, EXP2, or PTEX150 antibodies. RON3, KAHRP, and EXP2 staining is shown in green, and RESA, MAHRP1, and PTEX150 staining is shown in red. The nuclei staining (4′,6′-diamidino-2-phenylindole [DAPI]) is shown in blue. MAHRP1, KAHRP, or RESA was exported into the DMSO-treated infected RBCs while they appeared to be around the rapamycin-treated parasite. All images are representative of the majority of parasites over several fields and/or of three independent experiments. DIC, differential interference contrast. Bars, 2 $\mu$m.

indicating failure of translocon function for protein export to the RBC (Fig. 3A and B). In addition, KAHRP, the electron-dense histidine-rich protein that normally localizes to below the knobs on the RBC surface, and MAHRP1, located at Maurer's clefts, remained close to the parasite and were not translocated to the erythrocyte cytoplasm (Fig. 3A). Further analysis with antibodies to other exported proteins showed that the rapamycin-treated parasites were incapable of exporting other parasite proteins (skeleton binding protein 1 [SBP1], histidine-rich protein 2 [HRP2], and *P. falciparum* erythrocyte membrane protein 1 [*Pf*EMP1]; Fig. S3). Furthermore, in addition to RESA, the PTEX translocon components, EXP2 and PTEX150 (Fig. 3A), were detected in both DMSO- and rapamycin-treated parasites. EXP2, alongside the other PTEX components, are found in the dense granules (18) and allow the export of proteins, such as RESA, in healthy (normal) parasites.

To examine whether loss of RON3 also interfered with import of molecules into parasitized cells (a function of EXP2 in a role independent of the PTEX complex [11]), an assay was devised to directly detect import of a labeled glucose analogue, 2-(*N*-(-7-nitrobenz-2-oxa-1,3-diazol-4-yl)amino)-2-deoxyglucose (2-NBDG). Cells were further stained with Hoechst 33342 (DNA marker) and MitoTracker Deep Red (mitochondrial marker), which allowed parasites to be identified. Study of 2-NBDG uptake was not interfered with by the use of these two markers as determined using fluorescent controls (Fig. S4). RON3-deficient intracellular parasites were observed to take up less glucose than control DMSO-treated counterparts (Fig. 4A and C). After invasion, glucose uptake into the parasite was significantly lower than glucose uptake into the DMSO control, as quantified by comparing the mean fluorescent intensity (MFI) of 2-NBDG in DMSO- and rapamycin-treated parasites, wherein the MFI of background 2-NBDG signal in the infected RBC was subtracted from the 2-NBDG MFI in the parasite (change in MFI

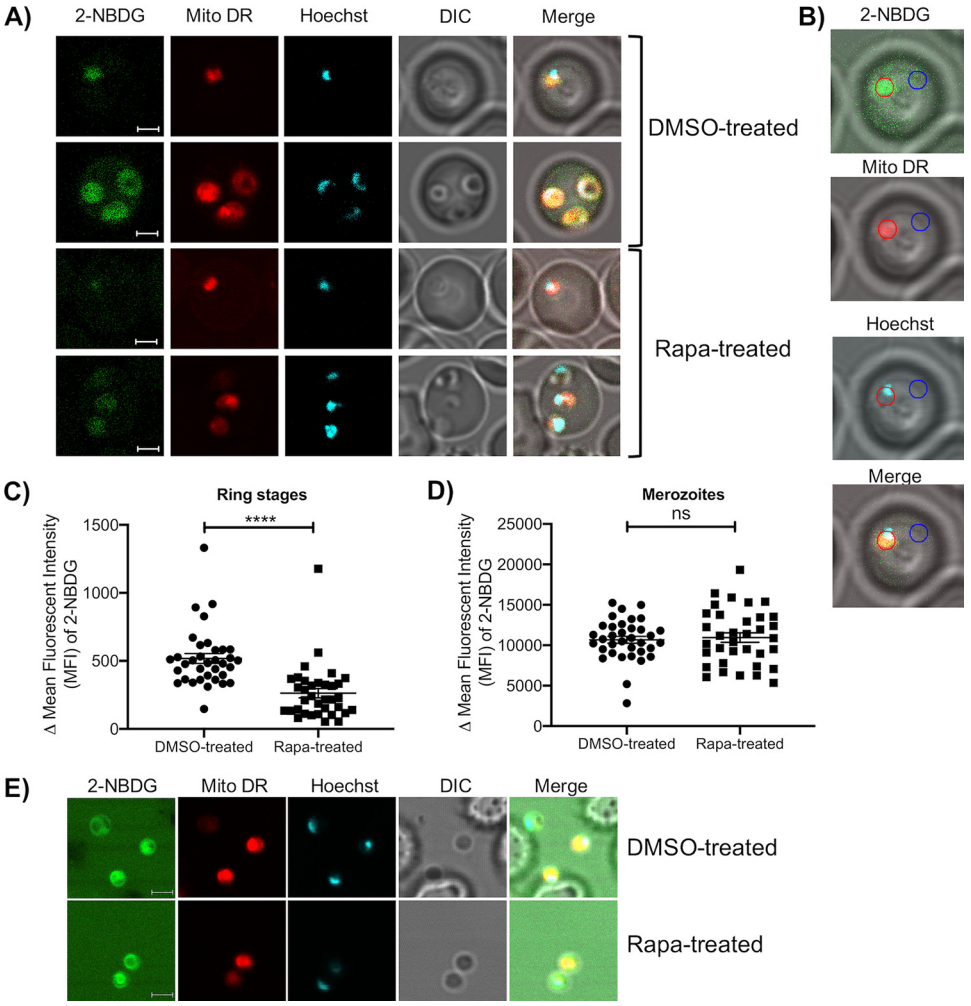


**FIG 4** Glucose uptake is decreased in *RON3loxP* parasites. The glucose analogue 2-NBDG was used to track glucose uptake into v2 cycle 2 DMSO- or rapamycin (Rapa)-treated parasites. (A) Representative images of DMSO- and Rapa-treated parasites after 2 h of incubation with 2-NBDG. Parasites were additionally stained with Hoechst 33342 (DNA marker) and MitoTracker Deep Red (Mito DR), a mitochondrial marker. Bars, 2 $\mu$m. (B) Example illustration of strategy for determining change in mean fluorescent intensity (ΔMFI) of 2-NBDG. MFI (green) was measured by first measuring fluorescent intensity attributed to the parasite (red circle as determined by localization with Hoechst/MitoTracker [blue/red] localization). Background MFI in the blood cell in which the parasite resides (blue circle) was subsequently subtracted to provide ΔMFI. (C) ΔMFI of 2-NBDG in DMSO-treated and rapamycin-treated ring-stage parasites ($n = 35$/group). (D) ΔMFI of 2-NBDG in DMSO-treated and rapamycin-treated merozoites was measured by subtracting background MFI from merozoite MFI. (E) Representative images of DMSO- and Rapa-treated merozoites stained with 2-NBDG ($n = 35$/group). Data represent the mean ± standard error of the mean (SEM). Statistical significance was determined by two-tailed unpaired *t* test where $P < 0.05$ is considered significant (****, $P < 0.0001$).

[ΔMFI]) (Fig. 4B). In two independent experiments (Fig. 4C and S5B), the ΔMFI of rapamycin-treated parasites was significantly less than that of the control, suggesting impairment of glucose uptake through the PVM. We further observed an outlier in the rapamycin-treated group; this is likely attributable to ~2% of parasites not undergoing excision during rapamycin treatment and has been previously observed in other DiCre mutants (14). As 2-NBDG is reported to metabolize to a nonfluorescent form, we repeated the experiment with a nonmetabolizable analogue, 6-NBDG (19), and found that DMSO-treated parasites still significantly took up more glucose than the rapamycin-treated parasites did (Fig. S5C). We further compared the background MFI of 2-NBDG or 6-NBDG in the infected blood cell (Fig. S5D) and found a significant difference between DMSO- and rapamycin-treated conditions. As demonstrated in this paper, the loss of RON3 leads to no parasite protein export through the PTEX translo-

con. The absence of these parasite proteins in the RBC may lead to reduced uptake in glucose by the infected RBC. However, as there is only ~20% reduction in uptake into the RBC between groups, we do not believe that this difference is enough to explain the ~50% reduction in glucose uptake into the RON3-deficient parasite.

To exclude a role for RON3 in the function of the hexose transporter (HT) that is located on the parasite plasma membrane (PPM), released merozoites that were treated with DMSO or rapamycin were investigated. Free rapamycin-treated merozoites were observed to take up glucose similarly to DMSO-treated parasites ($P > 0.05$; Fig. 4D), indicating that the HT present on the PPM is functional and exhibits similar activity.

## DISCUSSION

A major breakthrough in malarial cell biology was the identification of PTEX (2), a structure in the outer membrane of the PVM surrounding the intraerythrocytic parasite that transports proteins into the host erythrocyte membrane. The components of the translocon, including a pore-forming molecule, EXP2, are initially stored in the dense granules (18), which are structures located toward the apical end of the merozoite. During invasion, the dense granules release their contents in the space between the PPM and the invaginated RBC membrane (20), part of which is destined to become the PVM. Studies have since proven the function of components of the translocon by knockdown or destabilizing each of the different components of PTEX (3, 4). The electrophysiology of this vacuolar membrane was first studied by Desai et al. (9, 10) who estimated an upper limit to the size of molecules passing through pores in the membrane. Garten et al. (11) then confirmed these findings and identified this nutrient-permeable PVM channel as EXP2 by correlating its proteomic expression level with the probability of electrophysiological pore detection and by correctly predicting changes in physiological pore properties upon directed mutation of EXP2 as well as by demonstrating the permeability of the electrophysiological pore to small molecules which may then be imported into the parasite by transporters in the parasite plasma membrane. The critical study was the definition of its structure by cryo-electron microscopy that showed a plausible mechanism for the ATP-driven movement of proteins through the EXP2 pore (8).

Here we determined that another molecule, RON3, is critical for two distinct functions: export of parasite proteins into the RBC and import of small molecules, such as glucose, from the RBC to the parasite. The mechanism by which RON3 influences the function of PTEX remains to be elucidated, though we speculate that it may either have direct involvement with the translocon after insertion, play a role in translocon formation, or have an upstream effect. Evidence that suggests it is not related to sudden death of the parasite independent of the failure of function of the translocon is related to the following observations. First, merozoites invade RBCs normally after the loss of RON3, a complex series of events required by the parasite. Second, merozoites take up glucose equally in the DMSO- and rapamycin-treated parasites, indicative of a functional hexose transporter in the plasma membrane. Third, the PTEX translocon component EXP2 from the parasite's dense granules appeared to be released from the parasite although planned electron microscopy is needed to confirm this finding. Fourth, the parasite proteins investigated (KAHRP, MAHRP1, SBP1, *Pf*EMP1, and HRP2) are made in RON3-deficient parasites, although their export to the RBC does not occur. Using two distinct approaches to gene disruption of RON3, we show that the loss of RON3 causes the parasite to lose its PTEX function and arrest at an early stage of development. This is likely due to the limited availability of vital small molecules from the RBC, such as glucose.

Previous work identified *PfRON3* as an ortholog of *Toxoplasma gondii RON3* (*TgRON3*), a protein identified in the rhoptry proteome of *T. gondii* (12, 13). In *Plasmodium* spp., RON3 is found in the rhoptries (12), completely separate from the dense granules that house EXP2 and the other PTEX components (18). How RON3 functions after secretion and the mechanism by which it potentially affects the function of EXP2 or the translocon remains to be studied.

We can only speculate on the possible functional role of RON3 at this time; we are intrigued to note that the separation of RON3 and EXP2 would prevent both premature PTEX cargo discharge and premature dense granule hydration (often a consequence of ionic permeabilization of dense core secretory systems [e.g., mast cell granules {21}]). Failure to exocytose the rhoptries would likely halt invasion, and the failure of dense core granule fusion due to a lack of RON3 seems unlikely. Future imaging studies will examine the locations of RON3 after parasite entry.

Two of the predicted transmembrane domains within the RON3 sequence lie only a few amino acids apart (see Fig. S1 in the supplemental material). Unusually, all three transmembrane domains contain a single positively charged amino acid residue. Interestingly, *Tg*RON3 has just a single transmembrane domain that also contains a positively charged amino acid (13). This feature may facilitate the transfer of PTEX into the PVM or may have a functional role in protein export. In the original description of the PTEX translocon, RON3 (UniProt gene ID Q8I4R5, PlasmoDB ID PF3D7_1252100) was coimmunoprecipitated with PTEX150 tagged with hemagglutinin (PTEX150-HA) (2), but whether RON3 forms part of the translocon or is required for the formation of the translocon remains to be defined. The importance of RON3 in both translocon activity and glucose uptake expands the set of questions regarding the details of aspects of exocytosis, PVM permeability, translocon formation, and small-molecule transport.

## MATERIALS AND METHODS

**Reagents and antibodies.** Oligonucleotide primers were synthesized by Integrated DNA Technologies (Skokie, IL) or Sigma-Aldrich (St. Louis, MO). Rapamycin was obtained from Sigma-Aldrich and was prepared in dimethyl sulfoxide (DMSO) as a 50 $\mu$M stock. WR99210 was obtained from Jacobus Pharmaceuticals (Princeton, NJ) and stored as 20 $\mu$M stock in DMSO. 2-(*N*-(-7-nitrobenz-2-oxa-1,3-diazol-4-yl)amino)-2-deoxyglucose (2-NBDG), 6-(*N*-(-7-nitrobenz-2-oxa-1,3-diazol-4-yl)amino)-6-deoxyglucose (6-NBDG), MitoTracker Deep Red, and Hoechst 33342 were obtained from Thermo Fisher Scientific (Waltham, MA). 2-NBDG was stored as 14.6 mM stock in DMSO, 6-NBDG was stored as 5 mM stock solution, MitoTracker Deep Red was stored as 7.5 $\mu$M stock in DMSO, and Hoechst 33342 was stored as 20 mM stock solution. All restriction enzymes were obtained from New England Biolabs (Beverly, MA). Mouse RON3 antibodies (*Pf*RON3_1) were from Takafumi Tsuboi, Ehime University, Japan (12). Other antibodies were provided by Robin Anders, La Trobe University Australia (anti-RESA monoclonal antibody [Mab] 28/2) (22), Anthony Holder, The Francis Crick Institute, United Kingdom (UK) (anti-RON3 MAb 1H1), John Vakonakis, University of Oxford, UK (rabbit anti-MAHRP1) (23), Paul Gilson (rabbit anti-PTEX150) (24), and Diane Taylor, University of Hawaii USA (anti-KAHRP MAb 89) (25, 26). MAb 7.7, against EXP2, was from the European Malaria Reagent Repository, contributed by Jana McBride.

***P. falciparum* culture and transfection.** Transgenesis work used the *P. falciparum* 3D7-derived DiCre-expressing clone 1G5DiCre (14), also known as 1G5DC. Asexual blood-stage parasites were continuously cultured in complete medium (cRPMI; Roswell Park Memorial Institute [RPMI] 1640 medium containing Albumax [Gibco, Grand Island, NY]) and synchronized with 5% D-sorbitol (27). Transfection of 1G5DC was as previously described (28). Briefly, mature schizonts were enriched using Percoll (29) (GE Healthcare, Chicago, IL) and electroporated using an Amaxa 4D electroporator and P3 Primary cell 4D Nucleofector X kit L (Lonza, Basel, Switzerland) (14, 30). Drug selection with cRPMI supplemented with 2.5 nM WR99210 was initiated after 48 h posttransfection to allow selection of parasites transfected with plasmids carrying the human dihydrofolate reductase gene (*dhfr*) selectable marker. Integrant parasite clones for version 1 (v1) (3E10 and 7C4) and v2 (B11) were isolated by limiting dilution.

**Generation of *RON3loxP* parasites.** Generation of parasites with a floxed segment of genomic *RON3* gene was achieved by using CRISPR/cas9 gene editing. Two versions of the *RON3loxP* parasite were designed: version 1 (v1) replaced endogenous *RON3* exons 2 to 6 and introns 1 and 6 with recodonized exons 2 to 6 flanked by synthetic introns (*SERA2-loxPint* and *SUB2-loxPint*), and version 2 (v2) replaced endogenous *RON3* exons 6 and 7 and its flanking introns with recodonized exons 6 and 7 and synthetic *loxP* containing introns. A double transfection strategy was used, consisting of the dual Cas9- and sgRNA-encoding pDC2 plasmid (Marcus Lee, Sanger Institute) and a marker-free targeting plasmid (60 $\mu$g; pESS_RON3_v1_loxP or pESS_RON3_v2_loxP). All sgRNAs (20 $\mu$g each) were designed using EuPaGDT software (31) and generated by annealing complementary primer sequences. DiCre-mediated modification of *RON3loxP* version 2 (v2) parasites was confirmed by nucleotide sequencing before and after rapamycin treatment.

**Rapamycin treatment of *RON3loxP* parasites.** Recombination between the *loxP* sites was induced in synchronized ring-stage parasites by incubation with 100 nM rapamycin for 4 h; concurrently, parasites received mock treatment with DMSO (vehicle control). Rapamycin was washed out after 4 h with cRPMI, and parasites were allowed to progress to the next cycle.

**Diagnostic PCR detected excision, and sequencing of *RON3loxP*.** DiCre-mediated excision of the floxed RON3 exons was detected by PCR analysis of schizont-stage genomic DNA. Genomic DNA (gDNA) was extracted from schizont-stage cultures treated with DMSO or rapamycin (approximately 42 h after treatment) using Quick-gDNA MiniPrep (Zymo Research, Irvine, CA) or DNeasy Blood and Tissue kit

(Qiagen, Los Angeles, CA). PCR was conducted to determine excision events using 400 nM GoTaq Green Master Mix (Promega, Madison, WI) per the manufacturer's instructions, with appropriate primers. Fifteen-microliter PCRs were carried out in a thermocycler, and products were examined by SYBR Safe (ThermoFisher Scientific). Primers RON3_exon1_F (5′-AATGGTATAAGCGGTCATTATACAGAAGGTAGG-3′) and RON3_exon7_R (5′-ACAAGTTGTGATGTTTGTAACCTATGGG-3′) were used to detect excision events in v1, and RON3_exon5_F (5′-TCATACAGAAAAATATACAGT) and RON3_exon 8_R (5′-TCTCTTTTCAACTCTT TTTT-3′) were used to detect excision event in v2. The purified PCR product of v2 was capillary sequenced with Big-Dye terminator chemistry on an ABI3730xl DNA sequencer (Applied Biosystems, Foster City, CA).

**Growth and invasion analysis of *RON3loxP*.** Comparison of growth in v1 and v2 *RON3loxP* parasites treated with DMSO or rapamycin was determined by microscopy of Giemsa-stained thin blood films. For differential counts, a minimum of 1,000 cells were counted for each time point. Invasive capacity of v1 *RON3loxP* parasites was determined using a previously described method (32). Briefly, highly synchronous mature schizonts were Percoll purified (29) and then added to RBCs to a parasitemia of 1%. After 4 h, the cultures were fixed, enabling the percentage of newly ring-infected RBCs to be determined by Hoechst staining and analysis by flow cytometry (LSR II [BD Biosciences, San Jose, CA]). Samples were analyzed using FlowJo software.

**Indirect immunofluorescence assays.** Indirect immunofluorescence assays (IFAs) were conducted using *RON3loxP* v1 (clone 7C4) and v2 (clone B11). For v1 parasites, thin blood films of *RON3loxP* clone 7C4 parasites were air dried and stored at −80°C. The smears were thawed at 37°C and fixed in 4% paraformaldehyde (PFA) (Electron Microscopy Sciences, Hatfield, PA) for 30 min at room temperature. The cell membranes were permeabilized with 0.1% Triton X-100 (Sigma-Aldrich) in phosphate-buffered saline (PBS), for 10 min at room temperature and washed three times in PBS. The slides were blocked in 3% bovine serum albumin (BSA) in PBS for 2 h at room temperature and probed with mouse anti-RON3 (MAb 1H1; 1:100), mouse anti-RESA (1:1,000), mouse anti-KAHRP (1:500), anti-MAHRP1 (1:2,000), anti-EXP2 (MAb 7.7; 1:100), or anti-PTEX150 (1:100) for 1 h at room temperature. The slides were washed three times in PBS and probed with 1:8,000 goat anti-mouse Alexa Fluor 488 or 594 for 1 h at room temperature. After three washes with PBS, the slides were mounted in ProLong Gold Antifade Mountant with DAPI (Invitrogen, Carlsbad, CA) and sealed with Cytoseal-60 (ThermoFisher Scientific). Images were captured at 100×/1.45 numerical aperture (NA) with a Nikon Eclipse Ni-E wide-field microscope with a Hamamatsu C11440 digital camera or at 63×/1.4NA with a Zeiss laser scanning microscope (LSM) 880 microscope (Zeiss, Oberkochen, Germany) with AiryScan. The captured images were automatically processed with the Zen software to enhance the optical resolution isometrically by ~1.8-fold.

For v2 parasites, thin smears were made on glass slides and air dried. The cells were fixed in 4% PFA for 10 min at room temperature and permeabilized in 0.1% Triton X-100 for 15 min at room temperature. The smears were blocked in 5% nonfat milk (LabScientific, Highlands, NJ) overnight at 4°C. The slides were incubated with mouse anti-*Pf*RON3_1 (1:250) or mouse anti-RESA (1:1,000) for 1 h at 37°C and washed three times for 5 min each time with PBS. This was followed by incubation with goat anti-mouse Alexa Fluor 488 (1:1,000 for anti-RON3) or goat anti-mouse Alexa 594 (1:2,000 for anti-RESA) (Life Technologies, Carlsbad, CA) at 37°C for 45 min. The smears were washed three times for 5 min each time with PBS and air dried. The slides were mounted in ProLong Gold Antifade Mountant with DAPI and viewed at 63×/1.4NA with a Zeiss LSM 880 microscope with AiryScan. The captured images were automatically processed with the Zen software to enhance the optical resolution isometrically by ~1.8-fold.

**Live imaging of glucose analogue uptake by *RON3loxP*.** Synchronized parasites treated with rapamycin or DMSO were allowed to mature and progress to the next cycle, at which time they were passed through a MACS LS column (Miltenyi Biotec, Auburn, CA) to remove remaining schizonts. Intracellular ring-stage parasites were stained with 100 $\mu$M 2-NBDG or 6-NBDG and 600 nM MitoTracker Deep Red for 2 h at 37°C, after which the cells were washed with phenol red-free cRPMI. The procedure for investigation of merozoites was conducted with the following differences: schizonts were purified from cultures and stained with 2-NBDG and MitoTracker Deep Red, which were not washed out after incubation for 2 h. Cells were dispensed at 0.06% hematocrit to Nunc Lab-Tek II eight-well chamber slides (ThermoFisher Scientific) coated with 0.01% poly-L-lysine (Sigma-Aldrich). Prior to imaging, Hoechst 33342 was added to wells at a final concentration of 2 $\mu$M. Cells were imaged by Zeiss LSM 880 (Zeiss, Oberkochen, Germany); the system was allowed to equilibrate during sample preparation to permit samples to be maintained at 37°C and an atmosphere of 5% $CO_2$ during imaging. Time between washing and imaging was kept between 15 and 20 min. Images were captured using a 63×/1.4NA plan-apochromatic objective lens, and intensity information was measured using the Zen software tools. Further, to account for potential loss of 2-NBDG signal due to metabolism to a nonfluorescent form over time (33), collection of images for each treatment condition were staggered by switching between wells containing DMSO or rapamycin-treated parasites every five images. DMSO-treated parasites were additionally stained with each individual dye to act as fluorescent controls (see Fig. S4 in the supplemental material). The captured images were processed and analyzed using the Zen software. Mean fluorescent intensity (MFI) was measured by first measuring fluorescent intensity attributed to the parasite (as determined by localization with Hoechst/MitoTracker). Background MFI in the blood cell, in which the parasite resides, was subsequently subtracted to provide the change in MFI (ΔMFI). All imaging parameters were kept the same during imaging and between duplicate experiments. For analysis of merozoite intensity, background MFI was measured in the area around the merozoite.

**Statistical analysis.** All quantitative data were statistically analyzed and graphed using GraphPad Prism 7 or 8 for Mac. Data are presented as means ± standard errors of means (SEM) or standard deviations (SD). For differential counts of blood stages, each stage (ring, trophozoite, or schizont) was

normalized using the total percentage parasitemia at each particular time point. Unpaired two-tailed *t* test was used to determine significant differences between groups, with $P < 0.05$ as the threshold for significance.

## SUPPLEMENTAL MATERIAL

Supplemental material for this article may be found at https://doi.org/10.1128/mBio.01460-19.

**FIG S1**, TIF file, 0.1 MB.

**FIG S2**, TIF file, 0.3 MB.

**FIG S3**, TIF file, 0.8 MB.

**FIG S4**, TIF file, 0.5 MB.

**FIG S5**, TIF file, 0.5 MB.

## ACKNOWLEDGMENTS

We thank Susan K. Pierce (NIH) for her valuable suggestions and critical reading of the manuscript; Robin Anders, Anthony Holder, John Vakonakis, Paul Gilson, Diane Taylor, and The European Malaria Reagent Repository via contribution from Jana McBride for generously providing antibodies; Munir Akkaya for providing 2-NBDG and advice for using 2-NBDG; and Marcus Lee for the gift of plasmid pDC2.

This work was supported by the Intramural Research Program of the Division of Intramural Research, National Institute of Allergy and Infectious Diseases and the Eunice Kennedy Shriver National Institute of Child Health and Human Development, NIH, by a Wellcome Trust/NIH PhD studentship to E.S.S. (013459/Z/14/Z), and by funding to M.J.B. from the Francis Crick Institute (https://www.crick.ac.uk/), which received its core funding from Cancer Research UK (FC001043; https://www.cancerresearchuk.org), the UK Medical Research Council (FC001043; https://www.mrc.ac.uk/) and the Wellcome Trust (FC001043; https://wellcome.ac.uk/).

E.S.S., M.G., J.Z., M.J.B., and L.H.M. were involved in conception of research. L.M.L., Y.A., E.S.S., M.J.B., and L.H.M. designed research. L.M.L., Y.A., E.S.S., J.B., and J.M. performed research. T.T. provided reagents. L.M.L., Y.A., E.S.S., J.B., J.M., and L.H.M. analyzed data. L.M.L., Y.A., and L.H.M. wrote the paper. All authors critically read and edited the manuscript.

## REFERENCES

1. Aikawa M, Miller LH, Johnson J, Rabbege J. 1978. Erythrocyte entry by malarial parasites. A moving junction between erythrocyte and parasite. J Cell Biol 77:72–82. https://doi.org/10.1083/jcb.77.1.72.
2. de Koning-Ward TF, Gilson PR, Boddey JA, Rug M, Smith BJ, Papenfuss AT, Sanders PR, Lundie RJ, Maier AG, Cowman AF, Crabb BS. 2009. A newly discovered protein export machine in malaria parasites. Nature 459:945–949. https://doi.org/10.1038/nature08104.
3. Beck JR, Muralidharan V, Oksman A, Goldberg DE. 2014. PTEX component HSP101 mediates export of diverse malaria effectors into host erythrocytes. Nature 511:592–595. https://doi.org/10.1038/nature13574.
4. Elsworth B, Matthews K, Nie CQ, Kalanon M, Charnaud SC, Sanders PR, Chisholm SA, Counihan NA, Shaw PJ, Pino P, Chan JA, Azevedo MF, Rogerson SJ, Beeson JG, Crabb BS, Gilson PR, de Koning-Ward TF. 2014. PTEX is an essential nexus for protein export in malaria parasites. Nature 511:587–591. https://doi.org/10.1038/nature13555.
5. Russo I, Babbitt S, Muralidharan V, Butler T, Oksman A, Goldberg DE. 2010. Plasmepsin V licenses *Plasmodium* proteins for export into the host erythrocyte. Nature 463:632–636. https://doi.org/10.1038/nature08726.
6. Boddey JA, Hodder AN, Gunther S, Gilson PR, Patsiouras H, Kapp EA, Pearce JA, de Koning-Ward TF, Simpson RJ, Crabb BS, Cowman AF. 2010. An aspartyl protease directs malaria effector proteins to the host cell. Nature 463:627–631. https://doi.org/10.1038/nature08728.
7. Spielmann T, Gilberger TW. 2010. Protein export in malaria parasites: do multiple export motifs add up to multiple export pathways? Trends Parasitol 26:6–10. https://doi.org/10.1016/j.pt.2009.10.001.
8. Ho CM, Beck JR, Lai M, Cui Y, Goldberg DE, Egea PF, Zhou ZH. 2018. Malaria parasite translocon structure and mechanism of effector export. Nature 561:70–75. https://doi.org/10.1038/s41586-018-0469-4.
9. Desai SA, Krogstad DJ, McCleskey EW. 1993. A nutrient-permeable channel on the intraerythrocytic malaria parasite. Nature 362:643–646. https://doi.org/10.1038/362643a0.
10. Desai SA, Rosenberg RL. 1997. Pore size of the malaria parasite's nutrient channel. Proc Natl Acad Sci U S A 94:2045–2049. https://doi.org/10.1073/pnas.94.5.2045.
11. Garten M, Nasamu AS, Niles JC, Zimmerberg J, Goldberg DE, Beck JR. 2018. EXP2 is a nutrient-permeable channel in the vacuolar membrane of *Plasmodium* and is essential for protein export via PTEX. Nat Microbiol 3:1090–1098. https://doi.org/10.1038/s41564-018-0222-7.
12. Ito D, Han ET, Takeo S, Thongkukiatkul A, Otsuki H, Torii M, Tsuboi T. 2011. Plasmodial ortholog of *Toxoplasma gondii* rhoptry neck protein 3 is localized to the rhoptry body. Parasitol Int 60:132–138. https://doi.org/10.1016/j.parint.2011.01.001.
13. Bradley PJ, Ward C, Cheng SJ, Alexander DL, Coller S, Coombs GH, Dunn JD, Ferguson DJ, Sanderson SJ, Wastling JM, Boothroyd JC. 2005. Proteomic analysis of rhoptry organelles reveals many novel constituents for host-parasite interactions in *Toxoplasma gondii*. J Biol Chem 280:34245–34258. https://doi.org/10.1074/jbc.M504158200.
14. Collins CR, Das S, Wong EH, Andenmatten N, Stallmach R, Hackett F, Herman JP, Muller S, Meissner M, Blackman MJ. 2013. Robust inducible Cre recombinase activity in the human malaria parasite *Plasmodium falciparum* enables efficient gene deletion within a single asexual erythrocytic growth cycle. Mol Microbiol 88:687–701. https://doi.org/10.1111/mmi.12206.
15. Riglar DT, Richard D, Wilson DW, Boyle MJ, Dekiwadia C, Turnbull L, Angrisano F, Marapana DS, Rogers KL, Whitchurch CB, Beeson JG, Cowman AF, Ralph SA, Baum J. 2011. Super-resolution dissection of coordi-

nated events during malaria parasite invasion of the human erythrocyte. Cell Host Microbe 9:9–20. https://doi.org/10.1016/j.chom.2010.12.003.
16. Perlmann H, Berzins K, Wahlgren M, Carlsson J, Bjorkman A, Patarroyo ME, Perlmann P. 1984. Antibodies in malarial sera to parasite antigens in the membrane of erythrocytes infected with early asexual stages of *Plasmodium falciparum*. J Exp Med 159:1686–1704. https://doi.org/10.1084/jem.159.6.1686.
17. Favaloro JM, Coppel RL, Corcoran LM, Foote SJ, Brown GV, Anders RF, Kemp DJ. 1986. Structure of the RESA gene of *Plasmodium falciparum*. Nucleic Acids Res 14:8265–8277. https://doi.org/10.1093/nar/14.21.8265.
18. Bullen HE, Charnaud SC, Kalanon M, Riglar DT, Dekiwadia C, Kangwanrangsan N, Torii M, Tsuboi T, Baum J, Ralph SA, Cowman AF, de Koning-Ward TF, Crabb BS, Gilson PR. 2012. Biosynthesis, localization, and macromolecular arrangement of the *Plasmodium falciparum* translocon of exported proteins (PTEX). J Biol Chem 287:7871–7884. https://doi.org/10.1074/jbc.M111.328591.
19. Kim WH, Lee J, Jung DW, Williams DR. 2012. Visualizing sweetness: increasingly diverse applications for fluorescent-tagged glucose bioprobes and their recent structural modifications. Sensors (Basel) 12:5005–5027. https://doi.org/10.3390/s120405005.
20. Torii M, Adams JH, Miller LH, Aikawa M. 1989. Release of merozoite dense granules during erythrocyte invasion by *Plasmodium knowlesi*. Infect Immun 57:3230–3233.
21. Curran MJ, Brodwick MS. 1991. Ionic control of the size of the vesicle matrix of beige mouse mast cells. J Gen Physiol 98:771–790. https://doi.org/10.1085/jgp.98.4.771.
22. Brown GV, Culvenor JG, Crewther PE, Bianco AE, Coppel RL, Saint RB, Stahl HD, Kemp DJ, Anders RF. 1985. Localization of the ring-infected erythrocyte surface antigen (RESA) of *Plasmodium falciparum* in merozoites and ring-infected erythrocytes. J Exp Med 162:774–779. https://doi.org/10.1084/jem.162.2.774.
23. Oberli A, Slater LM, Cutts E, Brand F, Mundwiler-Pachlatko E, Rusch S, Masik MF, Erat MC, Beck HP, Vakonakis I. 2014. A *Plasmodium falciparum* PHIST protein binds the virulence factor *Pf*EMP1 and comigrates to knobs on the host cell surface. FASEB J 28:4420–4433. https://doi.org/10.1096/fj.14-256057.
24. Matthews K, Kalanon M, Chisholm SA, Sturm A, Goodman CD, Dixon MW, Sanders PR, Nebl T, Fraser F, Haase S, McFadden GI, Gilson PR, Crabb BS, de Koning-Ward TF. 2013. The *Plasmodium* translocon of exported proteins (PTEX) component thioredoxin-2 is important for maintaining normal blood-stage growth. Mol Microbiol 89:1167–1186. https://doi.org/10.1111/mmi.12334.
25. Rock EP, Marsh K, Saul AJ, Wellems TE, Taylor DW, Maloy WL, Howard RJ. 1987. Comparative analysis of the *Plasmodium falciparum* histidine-rich proteins HRP-I, HRP-II and HRP-III in malaria parasites of diverse origin. Parasitology 95:209–227. https://doi.org/10.1017/S0031182000057681.
26. Taylor DW, Parra M, Chapman GB, Stearns ME, Rener J, Aikawa M, Uni S, Aley SB, Panton LJ, Howard RJ. 1987. Localization of *Plasmodium falciparum* histidine-rich protein 1 in the erythrocyte skeleton under knobs. Mol Biochem Parasitol 25:165–174. https://doi.org/10.1016/0166-6851(87)90005-3.
27. Trager W, Jensen JB. 1976. Human malaria parasites in continuous culture. Science 193:673–675. https://doi.org/10.1126/science.781840.
28. Sherling ES, Knuepfer E, Brzostowski JA, Miller LH, Blackman MJ, van Ooij C. 2017. The *Plasmodium falciparum* rhoptry protein RhopH3 plays essential roles in host cell invasion and nutrient uptake. Elife 6:e23239. https://doi.org/10.7554/eLife.23239.
29. Rivadeneira EM, Wasserman M, Espinal CT. 1983. Separation and concentration of schizonts of *Plasmodium falciparum* by Percoll gradients. J Protozool 30:367–370. https://doi.org/10.1111/j.1550-7408.1983.tb02932.x.
30. Moon RW, Hall J, Rangkuti F, Ho YS, Almond N, Mitchell GH, Pain A, Holder AA, Blackman MJ. 2013. Adaptation of the genetically tractable malaria pathogen *Plasmodium knowlesi* to continuous culture in human erythrocytes. Proc Natl Acad Sci U S A 110:531–536. https://doi.org/10.1073/pnas.1216457110.
31. Peng D, Tarleton R. 2015. EuPaGDT: a web tool tailored to design CRISPR guide RNAs for eukaryotic pathogens. Microb Genom 1:e000033. https://doi.org/10.1099/mgen.0.000033.
32. Moss DK, Remarque EJ, Faber BW, Cavanagh DR, Arnot DE, Thomas AW, Holder AA. 2012. *Plasmodium falciparum* 19-kilodalton merozoite surface protein 1 (MSP1)-specific antibodies that interfere with parasite growth *in vitro* can inhibit MSP1 processing, merozoite invasion, and intracellular parasite development. Infect Immun 80:1280–1287. https://doi.org/10.1128/IAI.05887-11.
33. Yoshioka K, Saito M, Oh KB, Nemoto Y, Matsuoka H, Natsume M, Abe H. 1996. Intracellular fate of 2-NBDG, a fluorescent probe for glucose uptake activity, in *Escherichia coli* cells. Biosci Biotechnol Biochem 60:1899–1901. https://doi.org/10.1271/bbb.60.1899.